Astronomy & Astrophysics manuscript no. output
December 16, 2020

Fundamental properties of a selected sample of Ap stars: Inferences from interferometric and asteroseismic constraints

M. Deal[1], M. S. Cunha[1], Z. Keszthelyi[2], K. Perraut[3], and D. L. Holdsworth[4]

[1] Instituto de Astrofísica e Ciências do Espaço, Universidade do Porto CAUP, Rua das Estrelas, PT4150-762 Porto, Portugal
[2] Anton Pannekoek Institute for Astronomy, University of Amsterdam, Science Park 904, 1098 XH, Amsterdam, The Netherlands
[3] Univ. Grenoble Alpes, CNRS, IPAG, 38000 Grenoble, France
[4] Jeremiah Horrocks Institute, University of Central Lancashire, Preston PR1 2HE, UK
e-mail: morgan.deal@astro.up.pt

December 16, 2020

ABSTRACT

Context. Magnetic fields influence the formation and evolution of stars and impact the observed stellar properties. Ap stars are a prime example of this. Access to precise and accurate determinations of their stellar fundamental properties, such as masses and ages, is crucial to understand the origin and evolution of fossil magnetic fields.
Aims. We propose to use the radii and luminosity determined from interferometric measurements, in addition to seismic constraints when available, to infer as unbiased as possible fundamental properties of the 14 Ap stars characterized by Perraut et al. (2020).
Methods. We use a grid-based modelling approach, with stellar models computed with the CESTAM stellar evolution code, and the parameter search performed with the AIMS optimization method. The stellar models gird was built using a wide range of initial helium abundances and metallicities in order to avoid any bias coming from the initial chemical composition. The large separations ($\Delta\nu$) of HD 24712 and HD 128898 (2 roAp stars of the sample) were used as seismic constraints.
Results. We inferred the fundamental properties of the 14 stars in the sample. Most of the results are consistent within 1σ with those of Kochukhov & Bagnulo (2006), but a trend towards a slightly underestimated mass is visible in the results of these authors, due to the narrower initial chemical composition range considered in their grid, compared to ours. We show that the use of $\Delta\nu$ in the modelling significantly improves our inferences, allowing us to set reasonable constraints on the initial metallicity which is, otherwise, unconstrained. In particular, for HD 24712, we find a [Fe/H] value that is consistent with the iron abundance observed at the bottom of the photosphere, as determined by Shulyak et al. (2009).

1. Introduction

Magnetism is ubiquitously present on various scales in the Universe. Magnetic fields have a significant impact on star formation (e.g., Commerçon et al. 2011; Mackey & Lim 2011), as well as stellar structure and evolution (e.g., Mestel 1999; Donati & Landstreet 2009). The first stellar magnetic field of a star other than the Sun was detected by Babcock (1947). This star, 78 Vir, is a chemically-peculiar A-type star (Ap star). Consequently, research of Ap stars has a long and rich history (e.g., Babcock 1958; Wolff 1967, 1968; Landstreet 1982; Aurière et al. 2007; Sikora et al. 2019). They amount to only a few per cent of the A-type-star population (Power et al. 2007), yet their observation and modelling has a significant scientific potential. Ap star characterisation, both on a star-by-star basis and in terms of their ensemble properties, provides clues to the origin of strong, large-scale, fossil stellar magnetic fields (e.g., Cowling 1945; Braithwaite & Spruit 2017; Cantiello & Braithwaite 2019, and references therein), and can contribute to our understanding of how these fields influence both stellar evolution (e.g., Keszthelyi et al. 2019; Schneider et al. 2020) and the physical processes leading to the segregation of chemical elements via atomic diffusion (e.g. Michaud et al. 2015; Kochukhov & Ryabchikova 2018). Unfortunately, despite their scientific interest, Ap stars are not easy to characterise. In fact, classical stellar parameters of Ap stars derived from the analysis of photometric and/or spectroscopic data can be biased due to the surface chemical peculiarities. This, in turn, can lead to inaccurate determinations of the stars' fundamental properties, such as the mass, radius and age, compromising tests to our theoretical understanding of how these stars evolve and become chemically peculiar. In this context, the study of stars for which one may hope to derive unbiased classical parameters and fundamental properties, becomes particularly relevant. An example of such benchmarks are stars whose angular diameter can be directly measured through interferometry. With this in mind, over the past years an effort has been made to observe all Ap stars within reach of currently available interferometric instruments (Bruntt et al. 2008, 2010; Romanovskaya et al. 2019; Perraut et al. 2011, 2013, 2015, 2016, 2020). Together with state-of-the-art parallaxes and bolometric fluxes, the measured angular diameters were used to infer nearly model-independent radii, luminosities, and effective temperatures for this sample of benchmark Ap stars. The properties of the full sample, composed of 14 Ap stars, have recently been discussed by Perraut et al. (2020).

Among the Ap stars, there is a subgroup known as the rapidly oscillating Ap stars (hereafter, roAp stars) which exhibit high frequency pulsations (Kurtz 1982). Their effective temperatures range from about 6000 to 9000 K and their pulsation periods from about 5 min (Cunha et al. 2019) to 24 min (Alentiev et al. 2012). Up to now, most roAp stars have been discovered through the analysis of ground-based photometric time series, but the NASA TESS (Transiting Exoplanet Survey Satellite) is rapidly increasing the number of new detections (Cunha et al. 2019; Balona et al. 2019). The combination of interferometric and asteroseimic data has significant constraining power in the context

of stellar modelling (Cunha et al. 2007), making roAp stars with measured angular diameter primary targets for modelling.

The aim of the present paper is to use the interferometric radii and luminosities of the 14 stars characterized by Perraut et al. (2020) to infer their masses and ages. Within these 14 stars, 5 are roAp stars. The inference is performed with the grid-based optimization method AIMS (Asteroseismic Inference on a Massive Scale, Rendle et al. 2019). The stellar models are computed with the CESTAM evolution code (Code d'Evolution Stellaire Adaptatif et Modulaire, the "T" stands for Transport). To perform inferences as unbiased as possible, the grid includes various initial chemical compositions. In addition to radii and luminosities, we assess the benefit of having seismic constraints, when available. In order to further strengthen the robustness of these results, we additionally use the MESA software (Paxton et al. 2011, 2013, 2015, 2018, 2019) where the effects of surface fossil magnetic fields have previously been implemented by Keszthelyi et al. (2019, 2020).

In Section 2, we present the Ap stars sample and the information provided by roAp pulsations to constrain stellar models. The stellar models used to infer stellar parameters are described in Section 3 and the optimization procedure in Section 4. We present the inferred masses, ages and hydrogen mass fraction in the core (X_c) using classical and seismic constraints in Section 5. We finally discuss the results and address the impact of neglecting the magnetic field in Section 6 and conclude in Section 7.

2. Ap stars sample

2.1. Properties of the sample

This study focuses on the stars characterized by Perraut et al. (2020). The sample is composed of 14 Ap stars with angular diameters measured through interferometry (5 of them are roAp stars). They were chosen for the interferometry programme because they are brighter than the current sensitivity limit of visible interferometers, set in a magnitude range of about 8-8.5 in the R band (Ireland et al. 2008; Ligi et al. 2013), and have estimated angular diameters greater than about 0.2 mas, thus within the current angular resolution of these instruments. Information on the individual stars is given in Table 1, where the effective temperature, luminosity, and radius were extracted from table 4 of the paper by Perraut et al. (2020). For each star, the authors derived these properties from the angular diameter, bolometric flux, and parallax. The adopted parallaxes were retrieved from the GAIA DR2 (Gaia Collaboration et al. 2018) for all stars except for the two brightest targets, namely, HD 128898 and HD 137909 (the latter being a binary) for which the authors adopted, instead, the parallaxes from Hipparcos (van Leeuwen 2007). The bolometric flux was computed from the observed spectral energy distribution obtained by combining photometric and flux-calibrated spectroscopic data at different wavelengths. Figure 1 shows the stars in an Hertzsprung-Russell diagram along with evolutionary tracks and iso-radii, for different initial chemical compositions. Models are computed with the CESTAM evolution code using the input physics as described in Section 3. A core overshoot of 0.15 Hp is adopted for these tracks.

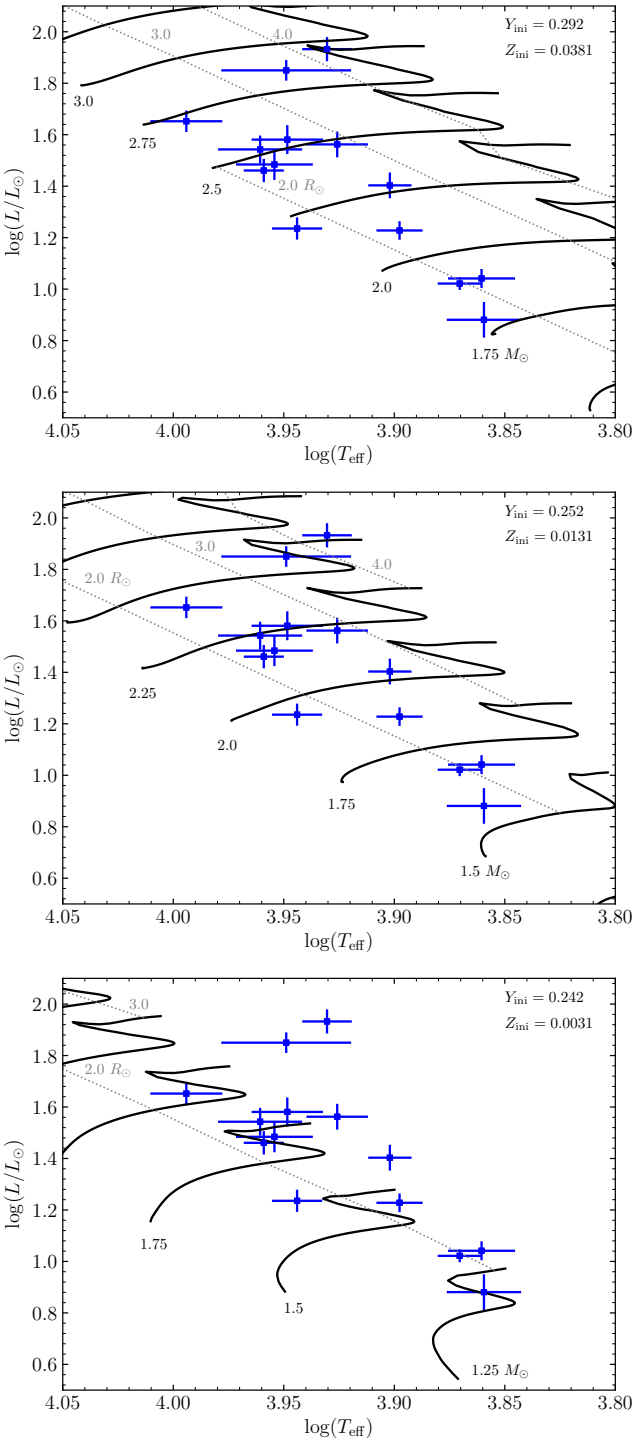

Fig. 1. HR diagram including the studied stars (blue symbols) listed in Table 1 and evolutionary tracks for masses between 1.25 and 3.25 $M_\odot$ at different initial chemical composition (black solid lines). The dotted lines represent the iso-radius at 2.0, 3.0 and 4.0 $R_\odot$. See the text for details about the models.

2.2. Seismology of Ap stars

The roAp stars have an added valuable scientific potential, as their pulsations may provide additional constraints to stellar modelling. Unfortunately, the strong magnetic field permeating the roAp stars distorts the pulsations and perturbs the pulsation frequencies with respect to those expected in non-magnetic stars. Studies of the interaction between the magnetic field and pulsations have shown that frequencies can be perturbed by a significant fraction of the typical frequency separation between consecutive modes (Cunha & Gough 2000; Cunha 2006; Bigot et al. 2000; Saio & Gautschy 2004). While the results from these theoretical studies agree qualitatively, quantitatively they show sig-

Table 1. Properties of the Ap star sample. Radii, luminosities and effective temperatures are taken from Perraut et al. (2020). The large frequency separations are derived from the literature following the description given in the text.

HD	Other name	$T_{\rm eff}$ [K]	L [$L_\odot$]	R [$R_\odot$]	$\Delta\nu$ [μHz]	$\Delta\nu_{\rm mag}$ [μHz]
4778	GO And	9135 ± 400	34.9 ± 4.3	2.36 ± 0.12	-	-
24712$^{(*)}$	HR1217	7235 ± 280	7.6 ± 1.2	1.75 ± 0.05	67.76 ± 0.13	[64.8, 68.8]
108662	17 Com A	8880 ± 330	38.1 ± 4.9	2.59 ± 0.12	-	-
108945	21 Com	8430 ± 270	36.5 ± 4.2	2.82 ± 0.09	-	-
118022	78 Vir	9100 ± 190	28.9 ± 3.0	2.17 ± 0.06	-	-
120198	84 UMa	9865 ± 370	44.9 ± 4.3	2.28 ± 0.10	-	-
128898$^{(*)}$	α Cir	7420 ± 170	10.51 ± 0.60	1.967 ± 0.066	60.37 ± 0.03	[57.4, 61.4]
137909$^{(*)}$	β CrB	7980 ± 180	25.3 ± 2.9	2.63 ± 0.09	-	-
153882	V451 Her	8980 ± 600	70.8 ± 6.5	3.46 ± 0.37	-	
176232$^{(*)}$	10 Aql	7900 ± 190	16.9 ± 1.4	2.21 ± 0.08	-	-
188041	V1291 Aql	9000 ± 360	30.5 ± 4.2	2.26 ± 0.05	-	-
201601$^{(*)}$	γ Equ A	7253 ± 235	11.0 ± 0.93	2.11 ± 0.07	-	-
204411	HR8216	8520 ± 220	85.6 ± 9.2	4.23 ± 0.11	-	-
220825	κ Psc	8790 ± 230	17.2 ± 1.7	1.78 ± 0.03	-	-

Notes. $^{(*)}$ roAp stars.

nificant differences in what concerns the perturbation to individual modes, bringing into question the use of the magnetic models in direct comparisons with the individual frequencies observed in roAp stars. Nevertheless, the scenario is different when considering the large frequency separations, $\Delta\nu$, between consecutive modes of the same degree, l. With the exception of modes experiencing a very strong coupling with the magnetic field, the frequency perturbation is not expected to vary significantly from mode to mode: it generally increases slightly with frequency, with a mode-to-mode variation which typically does not exceed 2 μHz, occasionally decreasing by a fraction of a μHz. As a consequence, the mode frequencies in roAp stars still tend to follow a regular pattern, often being almost equally spaced in the power spectrum. When that is the case, the observed large frequency separation can be determined and used as an extra constraint in the modelling of the star based on non-magnetic models, so far as a small magnetic correction is subtracted from the observed value.

Among the 14 stars in our sample, 5 were known to be roAp stars prior to the launch of TESS (identified by the symbol $*$ in Table 1). We searched the 2-min cadence TESS observations of the stars in our sample in search for additional roAp pulsators. Of the 14 stars analysed in this work, six stars (HD 137909, HD 153882, HD 176232, HD 188041, HD 201601 and HD 220825) do not yet have TESS photometric observations. We analysed both the Simple Aperture Photometry (SAP) and the Pre-search Data Conditioning SAP (PDC_SAP) data to check for any signal injected to the data by the PDC pipeline. To search for rotational variations, we calculated a Fourier spectrum from 0-10 d^{-1} (0-0.12 mHz). In the search for pulsational variability, we iteratively pre-whitened the light curve in the low-frequency range (0-10 d^{-1}; 0-0.12 mHz) to the noise level at high frequency to remove any rotation signal and instrumental artefacts. This serves to make the noise characteristics white in the region where pulsations are usually found. Of the 8 stars with TESS data, we detected pulsational variability in 2 previously known roAp stars (HD 24712 and HD 128898) and rotational variability in seven (HD 204411 shows no variability). Thus, the TESS data available so far does not increase the number of known roAp stars in our sample.

All data considered, we find that only two roAp stars, namely HD 24712 and HD 128898, show a regular frequency pattern. For these two stars, we shall use the observed large frequency separation as an additional constraint to the modelling. Since the large frequency separation scales with the square root of the mean density, we expect this extra constraint, together with the interferometric radius, to improve our inference of the stellar mass.

HD 24712 was discovered to be a roAp star by Kurtz (1981). Its pulsation spectrum is well characterised from long photometric time series acquired both from the ground (e.g. Kurtz et al. 2005) and space (Balona et al. 2019). It shows a series of equally-spaced modes, along with at least one frequency that does not follow the same pattern, the latter having been interpreted as an example of a mode that is strongly coupled with the magnetic field (Cunha 2001; Kurtz et al. 2002). There is strong evidence that the equally spaced modes are of alternating even and odd degree, from which it is deduced that the large frequency separation corresponds to twice the separation between adjacent modes. The frequency separation between the main oscillation modes of HD 24712 is very similar in the works by Kurtz et al. (2005) and Balona et al. (2019). Nevertheless, the values published in these works still differ by more than the formal error that would be derived from each of them. Therefore, for our modelling we combine the results from the two publications as follows: for each of them we compute three estimates of $\Delta\nu$ from the frequencies ν_1 to ν_5 (where the notation follows that used in both works), by considering the combinations $\nu_3 - \nu_1$, $\nu_4 - \nu_2$, and $\nu_5 - \nu_3$. We then compute the average and the square root of the variance of the six estimates and use them as estimates for the value and the uncertainty, finding $\Delta\nu = 67.76 \pm 0.13\,\mu$Hz. In addition to this pure observational estimate of $\Delta\nu$, we consider a more conservative scenario that takes into account the potential impact of the magnetic field on the oscillations. From the discussion above, we know that our non-magnetic models may systematically underestimate the true $\Delta\nu$ by up to about 2 μHz and occasionally overestimate it by up to a fraction of a μHz. Consequently, in this second scenario, we relax the observational seismic constraint by allowing $\Delta\nu$ to vary within the interval [$\Delta\nu$-3.0,$\Delta\nu$+1.0].

HD 128898 was discovered to be a roAp star by Kurtz & Cropper (1981) and has also been a target of several ground-based and space-based campaigns. A detailed analysis of its oscillation power spectrum has been performed by (Bruntt et al. 2009) based on space-based data collected with the star tracker on board the Wide-field Infrared Explorer (*WIRE*) (Buzasi 2002) and ground-based data collected at the South African Astronomical Observatory. Recently, new space-based data, acquired by the satellites TESS and BRITE have been analysed by Weiss et al. (2020), confirming the detection of the three main frequencies reported by (Bruntt et al. 2009) (f_6, f_1 and f_7, according to the notation adopted in both works). Similarly to the case of HD 24712, these three modes are interpreted as being of alternating even and odd degrees, implying that $\Delta\nu$ corresponds to twice the separation between adjacent modes. To estimate the value of $\Delta\nu$ and its uncertainty we proceed as before. In the present case there are only three equally spaced modes and, thus, only one estimate of $\Delta\nu$ from each publication. Moreover, in the case of Weiss et al. (2020) we considered only the frequencies derived from the TESS data, since the S/N in the BRITE data was significantly lower. Taking the average and the square root of the variance of the values from the two publications we find $\Delta\nu = 60.37 \pm 0.03\mu$Hz. Finally, as discussed for HD 24712, in addition to this observational value, we will consider a second scenario to account for the effect of the magnetic field not included in our stellar models, allowing $\Delta\nu$ to vary in the interval [$\Delta\nu$-3.0,$\Delta\nu$+1.0]. The intervals of $\Delta\nu$ considered for the two stars with seismic constraints are summarized in Table 1.

3. Stellar models

The stellar models are computed with the CESTAM evolution code (Code d'Evolution Stellaire Adaptatif et Modulaire, the "T" stands for Transport). A detailed description of the code can be found in Morel & Lebreton (2008), Marques et al. (2013) and Deal et al. (2018). The code is able to take into account several non-standard transport processes of chemical elements (i.e. atomic diffusion including radiative accelerations) and the transport of angular momentum which may have a significant impact on the stellar parameter inference in non-magnetic stars (e.g. Deal et al. 2020). Despite this, accounting for chemical element transport in Ap stars is still a challenge. The effect of the magnetic field on transport processes is currently poorly modelled in stellar evolution codes. Moreover, a realistic transport of chemical elements (including atomic diffusion) currently requires the addition of a parametric turbulent diffusion coefficient in order to reproduce surface abundances of F and A-type stars (Richer et al. 2000; Richard et al. 2001; Michaud et al. 2011; Verma et al. 2019; Semenova et al. 2020). The parametrization of such turbulent diffusion coefficient is not possible in Ap stars because atomic diffusion can be strongly affected by magnetic fields (Alecian & Stift 2002, 2007; Stift & Alecian 2016; Alecian & Stift 2017, and reference theirin). Consequently, we decided to not take any of these processes into account in the models computed for this study. However, we estimate the impact of atomic diffusion and an additional parametrized transport process for HD 24712 in Section 5.3. Similarly, the effects of a magnetic field on the evolution were neglected. An assessment of the effect of this assumption on the final properties is presented in Section 6.5.

The models are computed from the PMS (Pre-Main Sequence) to a hydrogen mass fraction in the core of $X_c = 10^{-11}$, to cover a part of the sub-giant phase. We use the OPAL2005 equation of state (Rogers & Nayfonov 2002) and the OPAL95 opacity tables (Iglesias & Rogers 1996) complemented at low temperatures by the Whichita opacity data (Ferguson et al. 2005). Nuclear reaction rates are from the NACRE compilation (Angulo 1999) except for the $^{14}N(p,\gamma)^{15}O$ reaction, for which we use the LUNA rate (Imbriani et al. 2004). We use an AGSS09 initial mixture of metal (Asplund et al. 2009) with meteoritic abundances for refractory elements (Serenelli 2010). Convection is treated following the Canuto et al. (1996) formalism with a solar calibrated $\alpha_{\rm CGM} = 0.634$. Overshoot of the convective core is taken into account with a step extend of $\alpha_{\rm ovs} \times \min(Hp, r_{\rm cc})$ where $r_{\rm cc}$ is the radius of the Schwarzschild convective core. Atmospheres are computed in the Eddington grey approximation with no mass loss taken into account.

4. Optimization method

4.1. AIMS code

The AIMS[1] optimization code (Asteroseismic Inference on a Massive Scale, Lund & Reese 2018, Rendle et al. 2019) applies a Markov chain Monte Carlo (MCMC) approach in order to find a representative sample of stellar models that fit a given set of classic and seismic constraints. This sample is subsequently used to find the best-fitting values, error bars, and posterior probability distribution functions (PDFs) for the different stellar properties. In order to gain computation time, the AIMS code uses a precomputed grid of stellar models which includes global stellar properties such as mass and age, as well as pulsation spectra, and interpolates within this grid for each MCMC iteration. Interpolation is carried out using a multi-dimensional Delaunay tessellation between evolutionary tracks and a simple linear interpolation along evolutionary tracks. AIMS allows the inclusion of the large frequency separation as a constraint and computes the model value, $\Delta\nu_{\rm mod}$, using the radial modes available in the grid. The posterior distribution of stellar fundamental properties A taking into account observational constraints O is defined as (Bayes' theorem)

$$p(A|O) \propto p(O|A)p(A), \tag{1}$$

with the likelihood function

$$p(O|A) = \frac{1}{\sqrt{2\pi|C|}} \exp(-\chi^2_{\rm tot}/2), \tag{2}$$

where $p(A)$ are prior assumptions and C is the covariance matrix of the observed parameters. In this study we assume uniform priors for the stellar fundamental properties. When the large frequency separation is used as a constraint, the χ^2 has the following form:

$$\chi^2_{\rm tot} = \sum \chi^2_{\rm classical} + \chi^2_{\Delta\nu}, \tag{3}$$

with

$$\chi^2_i = \left(\frac{O_i - \theta_i}{\sigma_i}\right)^2, \tag{4}$$

where classical means non-seismic constraints ($T_{\rm eff}$, luminosity, etc). O_i, θ_i and σ_i are respectively the observed value, the model value and the observational uncertainty. Otherwise the likelihood is only the sum of the classical constraint contributions.

Table 2. Properties of the grid of stellar models used to infer the stellar parameters.

Variables	Range	Steps
M ($M_\odot$)	1.2 - 3.5	0.025
$Y_{\rm ini}$	0.242 - 0.292	0.01
$Z_{\rm ini}$	0.0031 - 0.0381	0.005
ovs (H_p)	0.0 - 0.2	0.05

4.2. Grid parameters

The grid of models is Cartesian and includes five dimensions, namely the age, the mass, the initial helium and metal content, and the amount of core overshoot. The details about the grid can be found in Table 2. It has been designed to characterize main sequence stars (minimum hydrogen mass fraction of hydrogen in the core $X_c = 10^{-11}$). The value of the mixing length parameter is fixed to the solar calibrated value $\alpha_{\rm CGM} = 0.634$. The initial helium and metal mass fractions are chosen to include the solar calibrated ones as models of the grid ($Y_{\rm ini,\odot} = 0.252$ and $Z_{\rm ini,\odot} = 0.0131$). The minimum helium is chosen to include the primordial value and goes slightly below to allow proper probability distributions. The metallicity range is chosen to obtain an [Fe/H] coverage between −0.5 and 0.5 dex. We chose to not include lower metallicities because these are not expected for Ap main-sequence stars. Both $Y_{\rm ini}$ and $Z_{\rm ini}$ vary freely, i.e. no enrichment law is taken into account, to prevent any bias from such assumption. The counter part is the large number of models to compute. The total number of evolutionary tracks in our grid is 21689, including about 6.6 million models (between 200 and 1200 per track, depending on the mass and chemical composition). Core overshoot is chosen to cover the typical values for this parameter in the considered range of mass (Claret & Torres 2019). Oscillation frequencies are computed for each model of the grid using ADIPLS (Christensen-Dalsgaard 2008) applying a fully reflective boundary condition ($\delta P = 0$) at the top of the atmosphere. This boundary condition ensures that the frequencies are computed up to the observed values, which are greater than the acoustic cutoff frequency in both stars for which seismic constraints are applied. These very high frequencies are observed in roAp stars because the magnetic field provides a mechanism for partial refraction of the modes at frequencies higher than the acoustic cutoff frequency (Sousa & Cunha 2008; Quitral-Manosalva et al. 2018).

4.3. Classical constraints

We used the radius and the luminosity as classical constraints. We do not consider the effective temperature, because the latter is directly related to the other two through the Stefan-Boltzmann law and does not add an independent constraint. A wide variety of probability distribution functions can be applied by AIMS. In what follows, we used normal distributions, truncated at 3σ, for the two classical constraints.

As discussed in Section 3, the stellar models we use to determine the stellar parameters include no transport of chemical element. As [Fe/H] can be strongly affected by magnetic fields (e.g. Shulyak et al. 2009), we cannot use it as classical constraint.

[1] https://lesia.obspm.fr/perso/daniel-reese/spaceinn/aims/

4.4. Seismic constraints

We use the large frequency separations observed in HD 24712 and HD 128898 to improve the fits and assess the effect this additional constraint has on the probability distributions of the inferred stellar fundamental properties. Following on the discussion in Section 2.2, we consider two different scenarios. First we employ the constraint $\Delta\nu_{\rm mag}$, which incorporates a correction due the possible impact of the magnetic field. Under this scenario, we further consider two possibilities for the probability distribution of $\Delta\nu_{\rm mag}$, namely, a normal distribution with a central value of $(\Delta\nu - 1.0)$ and standard deviation of 2.0 μHz (hereafter $\Delta\nu(a)$) and a uniform distribution with a range $[\Delta\nu - 3.0\ ;\ \Delta\nu + 1.0]$ μHz (hereafter $\Delta\nu(b)$). The second scenario disregards the potential effect of the magnetic field, considering a normal distribution for the observed values $\Delta\nu_{\rm obs}$ (hereafter $\Delta\nu(c)$).

5. Parameter inferences

5.1. Masses, X_c and ages from classical constraints

In this section we discuss the results of the parameter inferences with AIMS. Table 3 gives the masses, hydrogen mass fractions in the core (X_c) and the ages of the 14 stars. The corresponding probability density functions are presented in Appendix C. The probability density functions are not strictly normal and present an asymmetry (positive or negative depending on the parameter). The central values given in Table 3 are the medians of the distributions (i.e. the 50$^{\rm th}$ percentile). We define the asymmetric uncertainties at 1σ with the 16$^{\rm th}$ and 84$^{\rm th}$ percentile of the distributions.

Figure 2 (left panel) shows the mass and hydrogen mass fraction in the core (X_c) inferred for the stars of the sample. Taking into account the 1σ error bars, the stars have masses between 1.5 and 3.0 $M_\odot$. Most of the stars are in the first half of the main sequence with $X_c < 0.35$ and ages between 0.01 and 1.7 Gyr, except for HD 153882 and HD 204411 which seem to be close to the end of main sequence with respectively $X_c = 0.22^{+0.10}_{-0.11}$ and $X_c = 0.10^{+0.05}_{-0.07}$. The uncertainties on X_c for these stars are smaller than for the others because they are possibly subgiants and the minimum hydrogen mass fraction of the models in the grid is $X_c = 10^{-11}$. A more accurate inference of the stellar fundamental properties of HD 153882 and HD 204411 would require extending the grid into the subgiant phase.

The inferred ages should be interpreted as estimates only. The grid of models includes core overshoot, but neglects other processes that may significantly affect the lifetime of main-sequence stars. Studies of G and F-type stars using grid-based modelling and including acoustic seismic constraints show that atomic diffusion can impact the age of a star by up to 15% (Nsamba et al. 2018; Deal et al. 2020). Similar results were also found for A-type stars using gravity modes as constraints (Mombarg et al. 2020). The effect of rotation is also not taken into account in the models. The transport of chemical elements by rotation has a direct impact on the lifetime of a star on the main sequence. There is also a degeneracy between the effect of core overshoot and rotation on the stellar age (e.g. Maeder 2009). In this context, X_c is more reliable than age as it is a measure of the fraction of evolution on the main sequence.

5.2. Chemical composition

Our results show that the chemical composition of the stars under study is not constrained by the classical observations alone.

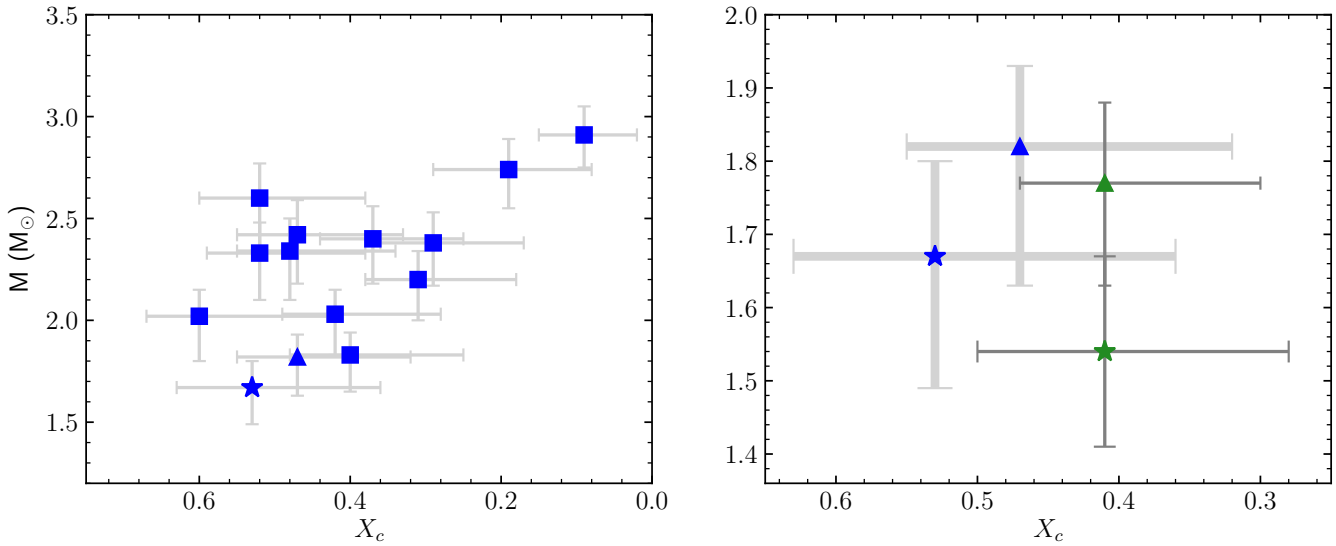

Fig. 2. *Left:* Inferred mass according to the inferred hydrogen mass fraction in the core (X_c) using the classical constraints, for the 14 stars of the sample (blue symbols). The star and pyramid symbols represent respectively HD 24712 and HD 128898. *Right:* Same as the left panel for HD 24712 and HD 128898 (blue symbols). Green symbols are the inferences when the $\Delta\nu(b)$ seismic constrain is taken into account.

There is a clear degeneracy both in the helium and metal contents. In the case of helium, we find that the probability density functions are homogeneous for all $Y_{\rm ini}$ values of the grid (see lower left panel of Fig. 3 for the example of HD 24712). For [Fe/H], the probability density functions are pointing towards the higher metallicities of the grid (see Appendix C) with no metallicities excluded (except, for HD 204411 for the reasons previously mentioned). This shape of the distribution of [Fe/H] is expected for a Cartesian grid (see Appendix A). It means that [Fe/H] is not constrained at all by the radius and luminosity.

The $Z_{\rm ini}$ probability density functions are not completely homogeneous and show an increasing trend towards high initial metal mass fraction (less pronounced than [Fe/H]) as shown on the lower middle panel of Fig 3 for HD 24712. Contrarily to [Fe/H], this is not expected. This comes from the architecture of the grid (all models are stopped at $X_c = 10^{-11}$), which was design to look for main sequence stars. At low metallicities, we can see on the bottom panel of Fig. 1 that the stars are at the edge of the tracks (outside for HD 153882 and HD 204411). This is the case at every $Y_{\rm ini}$. It means that there are less potential fitting models at lower than at higher metallicities, where all stars lie well within the evolutionary tracks. Note that we do not expect these young stars to have such low metallicities. We can thus consider $Z_{\rm ini}$, similarly to [Fe/H], completely unconstrained, taking into account the main sequence assumption.

5.3. Benefits from seismic constraints

For two stars of the sample (HD 24712 and HD 128898) we have a constraint on $\Delta\nu$, in addition to the radius and luminosity. Figure 3 shows the impact on the parameter inferences for HD 24712 of adding this seismic constraint, with uncertainties as described in Section 4.4. We can see that all three stellar properties are better constrained when the seismic information is considered, regardless of the type of uncertainties we use on $\Delta\nu_{\rm mag}$ (Gaussian or uniform, cases a and b, respectively). As expected, the constraining power of the seismic information increases when the more precise observed (uncorrected) value $\Delta\nu_{\rm obs}$, with smaller uncertainties, is adopted (case c). The values of the inferred masses, ages and X_c for the different cases considered for HD 24712 and HD 128898 are listed in Table 3. As expected, the main improvement brought by the seismic constraint is on the metal content. When $\Delta\nu$ is taken into account, the distribution in $Z_{\rm ini}$ (and in [Fe/H]) is better constrained. When uniform conservative uncertainties (cases b) are considered, we obtain 1σ intervals of $Z_{\rm ini} = 0.016^{+0.009}_{-0.007}$ and [Fe/H] $= 0.10^{+0.20}_{-0.23}$ dex for HD 24712, and $Z_{\rm ini} = 0.021^{+0.010}_{-0.009}$ and [Fe/H] $= 0.22^{+0.18}_{-0.25}$ dex for HD 128898. For all stellar properties, the improvement from adding the seismic constraint is more significant for HD 24712 than for HD 128898 (see Fig. B.1 of Appendix B for HD 128898). This is due to a smaller uncertainty on the luminosity for HD 128898, inducing a stronger constraint on the stellar fundamental properties without seismic constraint.

For comparison, we indicate on Fig. 3 (lower right panel) the value of [Fe/H] observed at the bottom of the photosphere by Shulyak et al. (2009) ($\log_{10}(N_{\rm Fe}/N_{\rm tot}) = -4.25$) using the solar iron abundance of Asplund et al. (2009) ($\log_{10}(N_{\rm Fe}/N_{\rm tot})_\odot = -4.5$) which gives [Fe/H]=0.25 dex. Our 1σ interval for [Fe/H] is in agreement with he observed iron abundance at the bottom of the photosphere. This indicates that using stellar models in which the transport of chemical elements is not taken into account, does not prevent from inferring realistic internal metallicities in this specific context.

As a test, we computed a model with the same evolution code (CESTAM), including the effect of atomic diffusion (with radiative acceleration) as described in Deal et al. (2018), and an additional parametrized transport process similar to what is expected in Am stars (e.g. Richer et al. 2000; Richard et al. 2001; Michaud et al. 2011). We used the median values obtained with the constrain of $\Delta\nu(b)$ and a free dYdZ to compute the model (M=1.54 $M_\odot$, $X_c = 0.39$ and $[{\rm Fe/H}]_{\rm ini} = 0.10$ dex). The models predict an increase of the abundance of iron at the bottom of the photosphere of about 0.5 dex. This is consistent with an initial [Fe/H] smaller than the current one (at the bottom of the photosphere), but the model surface abundance increase is too large compared to what we expect from the observed abundance. This indicates that the macroscopic transport of chemical elements may be more efficient in Ap stars than in Am stars. A detailed description of the

Table 3. Stellar parameters obtained with AIMS. Uncertainties are given at 1σ (16^{th} and 84^{th} percentiles).

	Free dYdZ			dYdZ = [0.4, 3.0]		
HD	Mass [$M_\odot$]	X_c	Age [Gyr]	Mass [$M_\odot$]	X_c	Age [Gyr]
4778	$2.41^{+0.17}_{-0.25}$	$0.45^{+0.09}_{-0.14}$	$0.38^{+0.19}_{-0.13}$	$2.39^{+0.15}_{-0.19}$	$0.45^{+0.08}_{-0.11}$	$0.38^{+0.16}_{-0.13}$
24712	$1.67^{+0.13}_{-0.18}$	$0.53^{+0.10}_{-0.17}$	$0.78^{+0.76}_{-0.47}$	$1.66^{+0.13}_{-0.16}$	$0.52^{+0.09}_{-0.15}$	$0.80^{+0.68}_{-0.45}$
$\Delta\nu(a)$	$1.55^{+0.13}_{-0.14}$	$0.41^{+0.10}_{-0.15}$	$1.29^{+0.60}_{-0.44}$	$1.56^{+0.12}_{-0.12}$	$0.42^{+0.09}_{-0.13}$	$1.20^{+0.59}_{-0.39}$
$\Delta\nu(b)$	$1.54^{+0.13}_{-0.13}$	$0.39^{+0.09}_{-0.13}$	$1.32^{+0.57}_{-0.40}$	$1.55^{+0.12}_{-0.12}$	$0.40^{+0.08}_{-0.11}$	$1.27^{+0.54}_{-0.36}$
$\Delta\nu(c)$	$1.58^{+0.11}_{-0.12}$	$0.43^{+0.08}_{-0.10}$	$1.19^{+0.35}_{-0.31}$	$1.57^{+0.10}_{-0.09}$	$0.43^{+0.07}_{-0.08}$	$1.17^{+0.33}_{-0.30}$
108662	$2.44^{+0.17}_{-0.24}$	$0.38^{+0.09}_{-0.13}$	$0.45^{+0.15}_{-0.11}$	$2.40^{+0.16}_{-0.19}$	$0.36^{+0.08}_{-0.11}$	$0.46^{+0.13}_{-0.11}$
108945	$2.38^{+0.16}_{-0.21}$	$0.29^{+0.08}_{-0.12}$	$0.56^{+0.13}_{-0.10}$	$2.37^{+0.13}_{-0.18}$	$0.28^{+0.07}_{-0.10}$	$0.56^{+0.12}_{-0.09}$
118022	$2.33^{+0.15}_{-0.23}$	$0.52^{+0.07}_{-0.14}$	$0.38^{+0.22}_{-0.13}$	$2.30^{+0.14}_{-0.18}$	$0.50^{+0.07}_{-0.10}$	$0.34^{+0.18}_{-0.13}$
120198	$2.60^{+0.17}_{-0.25}$	$0.53^{+0.08}_{-0.13}$	$0.24^{+0.15}_{-0.11}$	$2.57^{+0.16}_{-0.21}$	$0.52^{+0.08}_{-0.11}$	$0.24^{+0.13}_{-0.10}$
128898	$1.82^{+0.11}_{-0.19}$	$0.47^{+0.08}_{-0.15}$	$0.81^{+0.43}_{-0.25}$	$1.80^{+0.10}_{-0.14}$	$0.45^{+0.08}_{-0.11}$	$0.82^{+0.35}_{-0.24}$
$\Delta\nu(a)$	$1.77^{+0.12}_{-0.15}$	$0.42^{+0.07}_{-0.12}$	$0.97^{+0.30}_{-0.23}$	$1.76^{+0.11}_{-0.13}$	$0.41^{+0.06}_{-0.10}$	$0.95^{+0.27}_{-0.21}$
$\Delta\nu(b)$	$1.77^{+0.11}_{-0.14}$	$0.41^{+0.06}_{-0.11}$	$0.98^{+0.27}_{-0.19}$	$1.75^{+0.11}_{-0.12}$	$0.40^{+0.06}_{-0.09}$	$0.97^{+0.24}_{-0.20}$
$\Delta\nu(c)$	$1.80^{+0.09}_{-0.13}$	$0.44^{+0.05}_{-0.08}$	$0.91^{+0.23}_{-0.16}$	$1.77^{+0.10}_{-0.11}$	$0.43^{+0.05}_{-0.07}$	$0.90^{+0.22}_{-0.16}$
137909	$2.20^{+0.14}_{-0.20}$	$0.31^{+0.07}_{-0.13}$	$0.70^{+0.17}_{-0.13}$	$2.17^{+0.13}_{-0.17}$	$0.30^{+0.07}_{-0.11}$	$0.70^{+0.16}_{-0.12}$
153882	$2.80^{+0.15}_{-0.21}$	$0.22^{+0.10}_{-0.11}$	$0.41^{+0.07}_{-0.06}$	$2.77^{+0.14}_{-0.20}$	$0.22^{+0.12}_{-0.12}$	$0.39^{+0.08}_{-0.08}$
176232	$2.03^{+0.12}_{-0.20}$	$0.42^{+0.07}_{-0.14}$	$0.69^{+0.27}_{-0.17}$	$2.01^{+0.11}_{-0.17}$	$0.41^{+0.07}_{-0.11}$	$0.69^{+0.24}_{-0.17}$
188041	$2.34^{+0.16}_{-0.24}$	$0.48^{+0.07}_{-0.14}$	$0.39^{+0.21}_{-0.13}$	$2.32^{+0.15}_{-0.18}$	$0.47^{+0.06}_{-0.10}$	$0.38^{+0.16}_{-0.12}$
201601	$1.83^{+0.11}_{-0.18}$	$0.40^{+0.08}_{-0.15}$	$0.99^{+0.36}_{-0.24}$	$1.80^{+0.10}_{-0.16}$	$0.38^{+0.08}_{-0.12}$	$1.00^{+0.33}_{-0.24}$
204411	$2.93^{+0.14}_{-0.15}$	$0.10^{+0.05}_{-0.07}$	$0.43^{+0.06}_{-0.05}$	$2.89^{+0.14}_{-0.15}$	$0.09^{+0.05}_{-0.07}$	$0.44^{+0.07}_{-0.05}$
220825	$2.02^{+0.13}_{-0.22}$	$0.60^{+0.07}_{-0.17}$	$0.28^{+0.38}_{-0.20}$	$2.04^{+0.11}_{-0.14}$	$0.61^{+0.06}_{-0.10}$	$0.24^{+0.24}_{-0.16}$

effect of the magnetic field on the transport of chemical element can be found in Théado et al. (2005).

When only classical constraints are taken into account, the mass probability density functions of HD 24712 and HD 128898 indicate at 3σ a minimum mass of 1.21 and 1.28 $M_\odot$, respectively. It changes to 1.21 and 1.38 $M_\odot$ when $\Delta\nu$ with uniform uncertainty is considered. These masses are smaller than the current mass range typically assumed for Ap stars, which often starts in 1.5 $M_\odot$, based on the assumption of a solar chemical composition. The fact that the metallicity is largely unconstrained, leading to a significant uncertainty in the mass, indicates that the minimum mass of Ap stars may need to be shifted to lower values.

5.4. Enrichment law

An enrichment law characterizes the way the abundance of helium varies with the metallicity. It is suitable to study ensembles of stars but is less relevant for studies of individual stars, especially population I stars where the dispersion in this relation can be significant (e.g. Verma et al. 2019). This is the reason why we decided to not assume any enrichment law to start with. Nevertheless, we tested the impact of considering a constrained enrichment law. According to observations, the helium-to-heavy element enrichment ratio dY/dZ ranges between 0.4 and 3 (see Nsamba et al. 2020, for a review). The impact on the posterior distributions from constraining the value of dY/dZ can be seen in Table 3 and in Fig. 4. The median values for mass are slightly smaller when dY/dZ is constrained while remaining very close for X_c and age. As an additional constraint is taken into account, the 1σ uncertainties are smaller, as expected.

6. Discussion

6.1. Comparison with Kochukhov & Bagnulo (2006)

Fundamental stellar properties were determined for a large sample of Ap stars (including the 14 stars of this paper) by (Kochukhov & Bagnulo 2006, hereafter KB06). Masses and ages were derived using models with a unique initial metallicity $Z_{\rm ini} = 0.018$ (in interpolating in two grids with $Z_{\rm ini} = 0.008$ and 0.02). As shown in Fig. 5, our inferences are in agreement with theirs, taking into account our 1σ intervals, except for the mass of HD 204411 and the age of HD 108662 which are in agreement at 2σ (between the 5^{th} and 95^{th} percentiles of the probability density functions). On the other hand, our median values are not within their 1σ intervals for 9 stars out of 14. Our uncertainties are always larger. Despite the agreement within our uncertainties, we see that for 10 stars out of 14, KB06 inferences underestimate the masses compare to ours. The mean systematic differences normalized by each of the errors[2] are −0.39 and

[2] $1/14 \sum_i (M_{\rm KB06,}{}_i - M_i)/\sigma_i$

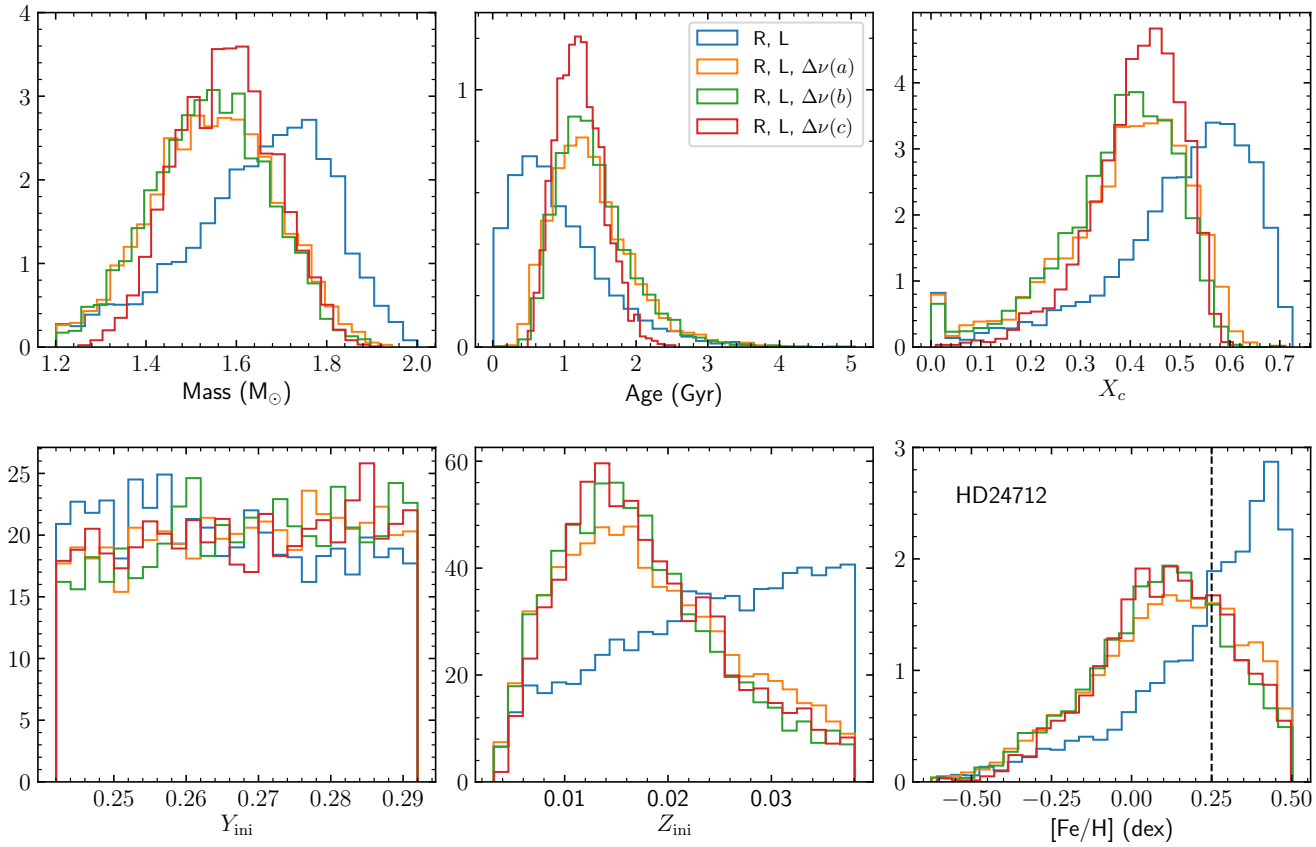

Fig. 3. Probability density functions for the mass, age, X_c, Y_{ini}, Z_{ini} and [Fe/H] of HD 24712. The blue distributions take into account the classical constraints only, while the orange, green and red ones include $\Delta\nu$ as an additional constraint with different uncertainties (see Section 4.4). The vertical dashed line is the observed [Fe/H] at the bottom of the photosphere for HD 24712 (Shulyak et al. 2009). Note that the [Fe/H] is the initial one as no transport is taken into account in the models of the grid.

-1.75 taking into account the 1σ intervals from this study (mean of the asymmetric interval) and from KB06, respectively. This comes from the fact that we considered a wider range of initial chemical compositions. For the age, the systematic difference are -0.07 and 0.40, using the 1σ intervals from this study and from KB06, respectively.

6.2. HD 24712: Comparison with Cunha et al. (2003)

HD 24712 (HR1217) was previously modelled by Cunha et al. (2003) using seismic constraints, taking into account different input physics and initial chemical compositions. However, the authors did not perform a complete optimization analysis, exploring the parameter space in a systematic manner to find the best model fits and characterize the uncertainties in the inferred properties, as performed in our study. They considered masses in the range M=[1.40;1.65] $M_\odot$, initial helium mass fraction in the range Y_{ini}=[0.23;0.30], initial metal mass fraction in the range Z_{ini}=[0.005;0.019] and two values of core overshoot α_{ov}=0.0 and 0.25. They showed that the models that were consistent with the observed large frequency separation they considered ($\Delta\nu = 67.91 \pm 0.12\,\mu$Hz) were the models with the higher values of helium ($Y_{ini} \approx 0.30$) and the smaller values of metallicities ($Z_{ini} \approx 0.005 - 0.009$). The also demonstrated that the mixing length parameter and core overshoot amount have less impact of the inferred stellar parameters that the initial chemical composition.

Our determination of the mass for HD 24712, using $\Delta\nu$ with conservative uniform uncertainties ($1.54^{+0.13}_{-0.13}$ $M_\odot$) is in agreement with the mass range identified by Cunha et al. (2003). Our results show that the initial metallicity at 1σ ($Z_{ini} = 0.016^{+0.009}_{-0.007}$) is slightly larger than the one of Cunha et al. (2003), while we have no constraints on the initial helium content. This small discrepancy probably results mainly from the adoption of a different initial mixture of metals (Grevesse & Noels 1993 in their study compare to Asplund et al. 2009 in ours) and additional differences in the input physics.

6.3. HD 128898: Comparison with Bruntt et al. (2009) and Weiss et al. (2020)

HD 128898 (αCir) was previously characterized by Bruntt et al. (2009) and Weiss et al. (2020), using seismic constraints. They estimated a mass of 1.71 ± 0.03 $M_\odot$ and 1.52 ± 0.15 $M_\odot$, respectively. Our mass determination is in good agreement with that of Bruntt et al. (2009) and overlaps in the upper part of the 1σ interval with that of Weiss et al. (2020). Similarly to Cunha et al. (2003), these literature mass estimates were not performed with a complete optimization analysis and a proper exploration of the parameter space, as presented in this paper.

6.4. Evolutionary state of Ap stars

The possibility that a correlation may exist between the presence of a magnetic field and the stellar age is still a matter under de-

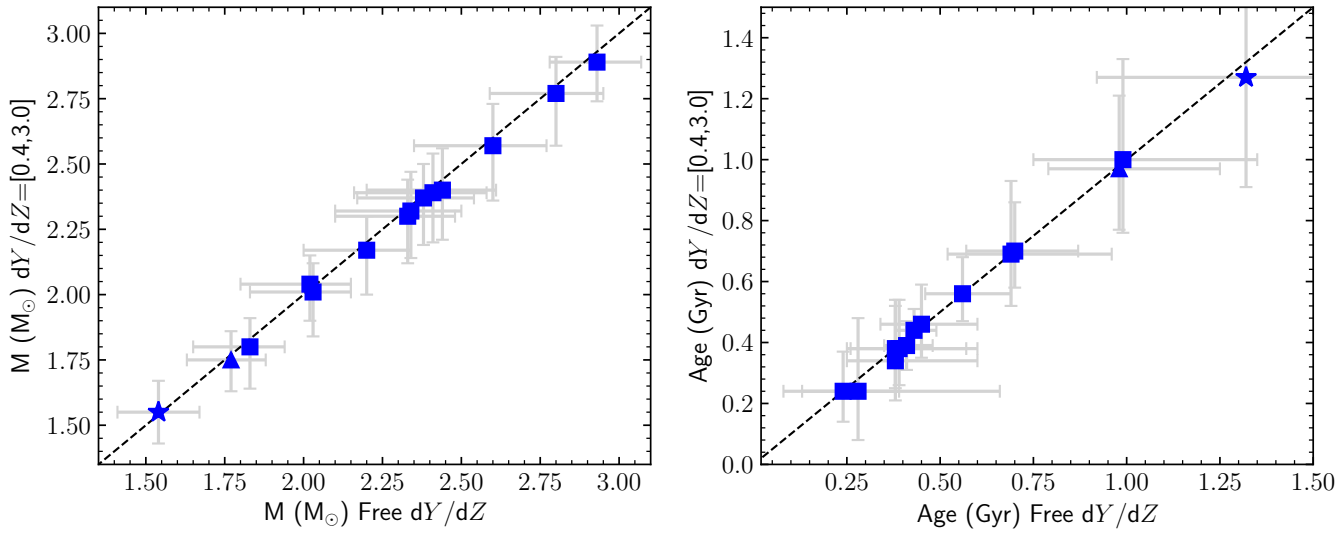

Fig. 4. Star-by-star comparison of the inferred mass (left panel) and age (right panel) using a free value of dY/dZ or an observationaly constrained one. The star and pyramid symbols represent respectively the properties for HD 24712 and HD 128898 inferred with the additional constraint $\Delta\nu(b)$. The dashed black lines are the 1:1 comparisons

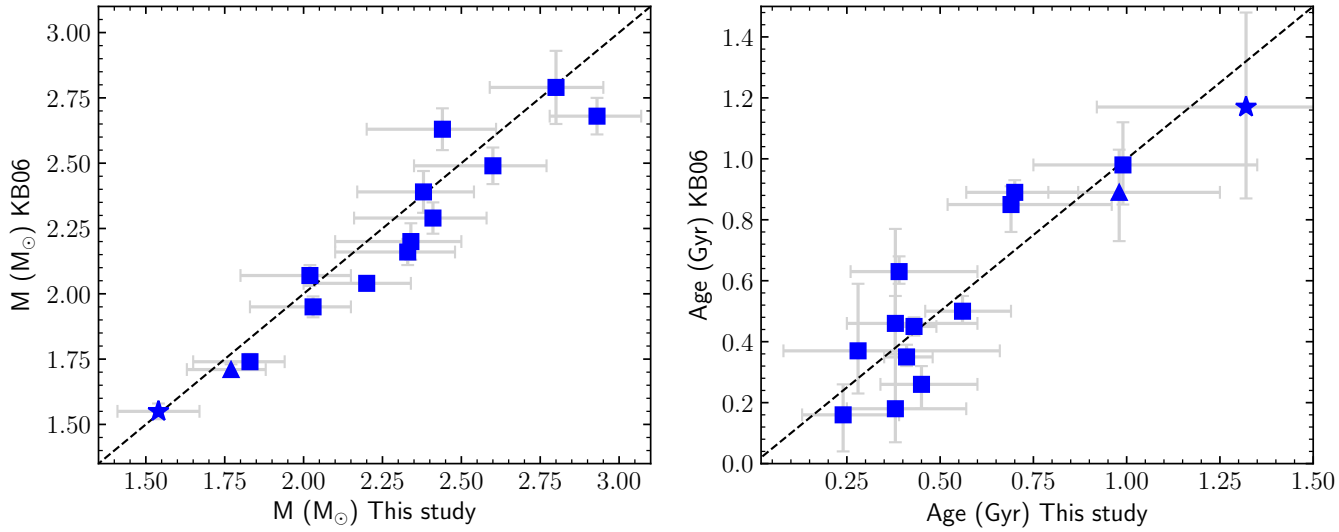

Fig. 5. Star-by-star comparison of the inferred mass (left panel) and age (right panel) from this study with Kochukhov & Bagnulo (2006). The star and pyramid symbols represent respectively the properties for HD 24712 and HD 128898 inferred with the additional constraint $\Delta\nu(b)$. The dashed black lines are the 1:1 comparisons.

bate. Hubrig et al. (2000) found that for stars with masses smaller than 3 $M_\odot$, magnetic fields only appear after they have spent about 30% of their lifetime on the main sequence. Later, other studies suggested that magnetic fields could appear earlier during the main sequence (Bagnulo et al. 2003; Kochukhov & Bagnulo 2006). In particular, using a significantly larger and less biased sample, KB06 found that 22 stars out of 125 with $M \leq 3\ M_\odot$ had a fractional age smaller than 0.3, rejecting the conclusion by Hubrig et al. (2000). Nevertheless, for stars with $M \leq 3\ M_\odot$, the authors found a tendency for clustering in the middle of the main sequence, which was even more evident when only stars with $M \leq 2\ M_\odot$ were considered. Figure 6 shows the fractional time on the main sequence for the 14 stars in our sample. We find that a large fraction of the stars in the sample have already spent at least 30% of their lifetime on the main sequence, reaching a maximum between 40 and 60%, consistent with the clustering around the middle of the main sequence found by KB06. Moreover, we find the youngest star (HD 220825) to have spent less than 20% of its lifetime on the main sequence, while 4 other stars have completed between 20 and 40% of their main sequence lifetime. Looking only at the stars in our sample, we find that our results predict, in average, smaller fractional times on the main sequence than those by KB06. This suggests that stars with magnetic fields could in average be even younger than expected from earlier works.

6.5. Impact of magnetic field

Recent modelling approaches[3] using the MESA software instrument have accounted for the surface effects of fossil magnetic

[3] https://doi.org/10.5281/zenodo.3250412
https://doi.org/10.5281/zenodo.3734209

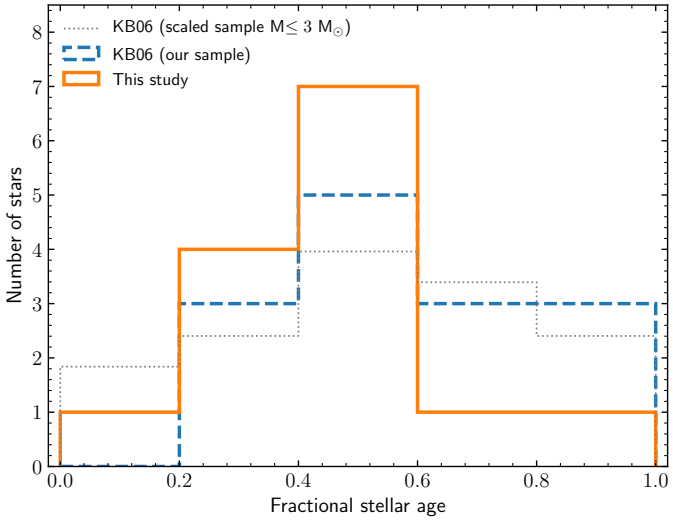

Fig. 6. Distribution of the relative ages of the stars in our sample according to this work (orange histogram) and to Kochukhov & Bagnulo (2006) (blue dashed histogram). We also show a scaled distribution from the full sample of Kochukhov & Bagnulo (2006) of stars with masses smaller or equal to 3 $M_\odot$ (grey dotted histogram).

fields in massive star models (Keszthelyi et al. 2019, 2020). These approaches rely on two long-term phenomena which result from the magnetospheric-wind interaction, namely, mass-loss quenching (which reduces the mass-loss rate of the star, e.g., ud-Doula & Owocki 2002; Bard & Townsend 2016) and magnetic braking (which reduces the rotation rate of the star, e.g., ud-Doula et al. 2008, 2009). Thus far such state-of-the-art models did not cover the mass range presented in this work. To this extent, we employ this modelling approach with the goal to determine how much these effects can modify the fundamental stellar properties of Ap stars. Of course, an important caveat is that in these models the internal magneto-hydrodynamical effects are not yet implemented for fossil fields, however, semi-analytical methods do exist (Mathis & Zahn 2005; Duez & Mathis 2010).

6.5.1. MESA model description

The modelling assumptions are similar to those of Keszthelyi et al. (2020). The initial abundances are adopted as $Z_{\rm ini} = 0.014$, $Y_{\rm ini} = 0.266$, $X_{\rm ini} = 0.72$, and the initial distribution of metals follows the description of Asplund et al. (2009), with isotopic ratios adopted from Lodders (2003). The convective mixing is adopted with $\alpha_{\rm MLT} = 1.8$ and the Ledoux criterion is used to determine the convective boundary. Overshooting is applied with the exponential method, with parameters $f = 0.021$ and $f_0 = 0.006$, which approximately corresponds to $\alpha_{\rm ovs} = 0.15$.

For simplicity, we adopt a mass-loss rate of 10^{-14} $M_\odot\,{\rm yr}^{-1}$ constant in time. Magnetic braking is modelled in the "uniform" scheme of Keszthelyi et al. (2020), considering that all layers of the star are torqued. Chemical mixing and angular momentum transport follow the usual MESA methods described by Paxton et al. (2013), and we do not include atomic diffusion.

Here, since we are interested in how much the surface effects of fossil magnetic fields modify the fundamental properties, we compute three sets of models in the mass range from 1.5 to 2.6 $M_\odot$. The first set is for zero rotation and zero magnetic field strength (labelled "V0B0"), the second is for an initial rotational velocity[4] of 90 km s^{-1} and zero field strength ("V90B0"), and the third is for an initial rotational velocity of 90 km s^{-1} and 6 kG magnetic field strength ("V90B6"). In the latter ones, the magnetic field weakens over time, following Alfvén's theorem of magnetic flux conservation.

6.5.2. MESA modelling results

Figure 7 shows the computed model diagnostics regarding their fundamental properties. In this mass range, the impact on the stellar luminosity is negligibly small (unlike higher-mass models, where complete evolutionary paths can be modified, see, e.g., Petit et al. 2017; Georgy et al. 2017).

The effective temperature and stellar radius differ in the case of rotating models, shifting the ZAMS location to lower $T_{\rm eff}$ and larger $R_\star$ (compared to non-rotating models) to find mechanical equilibrium. Rotating, non-magnetic models (grey dashed lines) would therefore evolve differently, affecting the diagnostics.

The models with rotation and an initial magnetic field strength of 6 kG (black dashed lines), however, spin down due to magnetic braking. Therefore, as shown in Figure 7, despite the initially different ZAMS position, they converge to the non-rotating models (Keszthelyi et al. 2019, 2020).

Considering various phases during the evolution, we find that the maximum difference in fundamental properties is 2 % when comparing non-rotating, non-magnetic models with rotating magnetic models with MESA. This is, of course, with the important provision that the magnetic models here concern only the above-mentioned surface effects. These findings strengthen the analysis and results with the CESTAM code (where the surface magnetic field effects are not yet implemented), underscoring that in this mass range we do not anticipate a significant shortcoming within the scope of this paper by using non-rotating and non-magnetic models.

7. Conclusion

We inferred the stellar fundamental properties of the 14 Ap stars (including 5 roAp stars) characterized by Perraut et al. (2020), using a grid-base modelling approach. We used the CESTAM stellar evolution code to compute the models and the AIMS optimization method to infer the stellar properties. The grid of models included a wide range of initial chemical compositions to avoid any assumptions, and derive as unbiased as possible stellar properties. Interferometric radii and luminosities were used as classical constraints. The properties we inferred are consistent with previous work (e.g. Kochukhov & Bagnulo 2006) but with larger error bars. They are more conservative due to the wider parameter space explored, especially in the initial chemical composition. Despite the agreement, we see a trend in Kochukhov & Bagnulo (2006) inferences towards lower masses for stars up to 0.2 $M_\odot$. This comes from the narrower range of initial chemical composition they considered (solar metallicity).

We considered two different choices for the initial chemical composition. Firstly, we let the variation of initial helium and metallicity free, which is more suitable for a star by star analysis. Secondly, we selected only models in which the variation of these two parameters were constrained by observations, which is suitable for ensemble analyses. In both scenarios, the inferred

[4] The mean $v \sin i$ of the sample is 30.5 km s^{-1} and the maximum is 75 km s^{-1} (see Royer et al. 2002 for all the stars except for HD 128898: Desidera et al. 2015 and HD 201601: Uesugi & Fukuda 1970), which makes 90 km s^{-1} a reasonable upper limit.

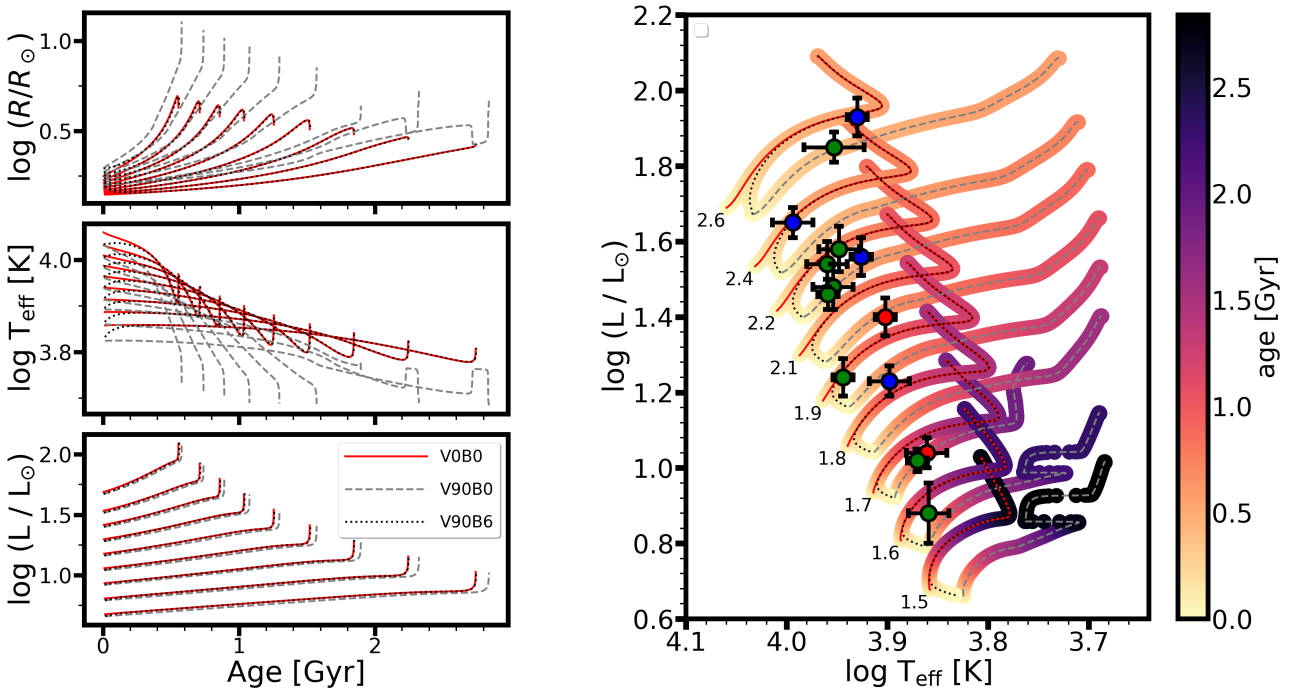

Fig. 7. Shown are three sets of MESA evolutionary models: with zero rotation and magnetic field strength (red solid lines), $v_{\rm ini}$ = 90 km s^{-1} and $B_{\rm ini}$ = 0 (grey dashed lines), and $v_{\rm ini}$ = 90 km s^{-1} and $B_{\rm ini}$ = 6 kG (black dotted lines). The 14 sample stars are colour-coded according to their measured magnetic field strengths as red (> 4 kG), green (2 kG < and < 4 kG), and blue (< 2 kG). The stellar mass in solar units is indicated next to the tracks on the right panel.

stellar properties were very similar. We also showed that the use of models that do not incorporate the effects of a magnetic fossil field and rotation does not significantly affect the inferred properties.

Our results suggest that stars with magnetic fields can be younger than what was expected from previous studies (Hubrig et al. 2000). We found that 5 of the 14 stars have spent less than 40% (below 20% for HD 220825) of their lifetime on the main sequence. Our results are in better agreement with the results of Bagnulo et al. (2003) and Kochukhov & Bagnulo (2006).

Finally, our study emphasises how knowledge of the large frequency separation $\Delta\nu$ provides an additional important constraint to the inference of the stellar properties, as illustrated by the study of the two roAp stars in our sample, HD 24712 and HD 128898. Most importantly, with the addition of $\Delta\nu$ it is possible to constrain the initial [Fe/H], as found for the case of HD 24712, for which we inferred a value which is consistent with the results from the abundances analysis of Shulyak et al. (2009). The use of seismic information thus opens new interesting possibilities to constrain the internal chemical composition and the transport of chemical elements in Ap stars.

Acknowledgements. MD acknowledges D. Reese for fruitful discussions and for the recent improvements of the AIMS optimization code used for this study. This work was supported by FCT/MCTES through the research grants UIDB/04434/2020, UIDP/04434/2020 and PTDC/FIS-AST/30389/2017, and by FEDER - Fundo Europeu de Desenvolvimento Regional through COMPETE2020 - Programa Operacional Competitividade e Internacionalização (grant: POCI-01-0145-FEDER-030389). MD and MSC are supported by national funds through FCT in the form of a work contract. DLH acknowledges financial support from the Science and Technology Facilities Council (STFC) via grant ST/M000877/1.

References

Alecian, G. & Stift, M. J. 2002, A&A, 387, 271
Alecian, G. & Stift, M. J. 2007, A&A, 475, 659
Alecian, G. & Stift, M. J. 2017, MNRAS, 468, 1023
Alentiev, D., Kochukhov, O., Ryabchikova, T., et al. 2012, MNRAS, 421, L82
Angulo, C. 1999, in American Institute of Physics Conference Series, Vol. 495, American Institute of Physics Conference Series, 365–366
Asplund, M., Grevesse, N., Sauval, A. J., & Scott, P. 2009, ARA&A, 47, 481
Aurière, M., Wade, G. A., Silvester, J., et al. 2007, A&A, 475, 1053
Babcock, H. W. 1947, ApJ, 105, 105
Babcock, H. W. 1958, ApJ, 128, 228
Bagnulo, S., Landstreet, J. D., Lo Curto, G., Szeifert, T., & Wade, G. A. 2003, A&A, 403, 645
Balona, L. A., Holdsworth, D. L., & Cunha, M. S. 2019, MNRAS, 487, 2117
Bard, C. & Townsend, R. H. D. 2016, MNRAS, 462, 3672
Bigot, L., Provost, J., Berthomieu, G., Dziembowski, W. A., & Goode, P. R. 2000, A&A, 356, 218
Braithwaite, J. & Spruit, H. C. 2017, Royal Society Open Science, 4, 160271
Bruntt, H., Kervella, P., Mérand, A., et al. 2010, Astronomy & Astrophysics, 512, A55
Bruntt, H., Kurtz, D. W., Cunha, M. S., et al. 2009, MNRAS, 396, 1189
Bruntt, H., North, J. R., Cunha, M., et al. 2008, Monthly Notices of the Royal Astronomical Society, 386, 2039
Buzasi, D. 2002, in Astronomical Society of the Pacific Conference Series, Vol. 259, IAU Colloq. 185: Radial and Nonradial Pulsationsn as Probes of Stellar Physics, ed. C. Aerts, T. R. Bedding, & J. Christensen-Dalsgaard, 616
Cantiello, M. & Braithwaite, J. 2019, ApJ, 883, 106
Canuto, V. M., Goldman, I., & Mazzitelli, I. 1996, ApJ, 473, 550
Christensen-Dalsgaard, J. 2008, Ap&SS, 316, 113
Claret, A. & Torres, G. 2019, ApJ, 876, 134
Commerçon, B., Hennebelle, P., & Henning, T. 2011, ApJ, 742, L9
Cowling, T. G. 1945, MNRAS, 105, 166
Cunha, M. S. 2001, MNRAS, 325, 373
Cunha, M. S. 2006, MNRAS, 365, 153
Cunha, M. S., Aerts, C., Christensen-Dalsgaard, J., et al. 2007, The Astronomy and Astrophysics Review, 14, 217
Cunha, M. S., Antoci, V., Holdsworth, D. L., et al. 2019, MNRAS, 487, 3523
Cunha, M. S., Fernandes, J. M. M. B., & Monteiro, M. J. P. F. G. 2003, MNRAS, 343, 831
Cunha, M. S. & Gough, D. 2000, MNRAS, 319, 1020
Deal, M., Alecian, G., Lebreton, Y., et al. 2018, A&A, 618, A10
Deal, M., Goupil, M. J., Marques, J. P., Reese, D. R., & Lebreton, Y. 2020, A&A, 633, A23
Desidera, S., Covino, E., Messina, S., et al. 2015, A&A, 573, A126
Donati, J. F. & Landstreet, J. D. 2009, ARA&A, 47, 333

Duez, V. & Mathis, S. 2010, A&A, 517, A58
Ferguson, J. W., Alexander, D. R., Allard, F., et al. 2005, ApJ, 623, 585
Gaia Collaboration, Brown, A. G. A., Vallenari, A., et al. 2018, A&A, 616, A1
Georgy, C., Meynet, G., Ekström, S., et al. 2017, A&A, 599, L5
Grevesse, N. & Noels, A. 1993, in Origin and Evolution of the Elements, ed. N. Prantzos, E. Vangioni-Flam, & M. Casse, 15–25
Hubrig, S., North, P., & Mathys, G. 2000, ApJ, 539, 352
Iglesias, C. A. & Rogers, F. J. 1996, ApJ, 464, 943
Imbriani, G., Costantini, H., Formicola, A., et al. 2004, A&A, 420, 625
Ireland, M. J., Mérand, A., ten Brummelaar, T. A., et al. 2008, in Society of Photo-Optical Instrumentation Engineers (SPIE) Conference Series, Vol. 7013, Optical and Infrared Interferometry, ed. M. Schöller, W. C. Danchi, & F. Delplancke, 701324
Keszthelyi, Z., Meynet, G., Georgy, C., et al. 2019, MNRAS, 485, 5843
Keszthelyi, Z., Meynet, G., Shultz, M. E., et al. 2020, MNRAS, 493, 518
Kochukhov, O. & Bagnulo, S. 2006, A&A, 450, 763
Kochukhov, O. & Ryabchikova, T. A. 2018, MNRAS, 474, 2787
Kurtz, D. W. 1981, Information Bulletin on Variable Stars, 1915, 1
Kurtz, D. W. 1982, MNRAS, 200, 807
Kurtz, D. W., Cameron, C., Cunha, M. S., et al. 2005, MNRAS, 358, 651
Kurtz, D. W. & Cropper, M. S. 1981, Information Bulletin on Variable Stars, 1987, 1
Kurtz, D. W., Kawaler, S. D., Riddle, R. L., et al. 2002, MNRAS, 330, L57
Landstreet, J. D. 1982, ApJ, 258, 639
Ligi, R., Mourard, D., Nardetto, N., & Clausse, J. M. 2013, Journal of Astronomical Instrumentation, 2, 1340003
Lodders, K. 2003, ApJ, 591, 1220
Lund, M. N. & Reese, D. R. 2018, Asteroseismology and Exoplanets: Listening to the Stars and Searching for New Worlds, 49, 149
Mackey, J. & Lim, A. J. 2011, MNRAS, 412, 2079
Maeder, A. 2009, Physics, Formation and Evolution of Rotating Stars
Marques, J. P., Goupil, M. J., Lebreton, Y., et al. 2013, A&A, 549, A74
Mathis, S. & Zahn, J.-P. 2005, A&A, 440, 653
Mestel, L. 1999, Stellar magnetism
Michaud, G., Alecian, G., & Richer, J. 2015, Atomic Diffusion in Stars
Michaud, G., Richer, J., & Vick, M. 2011, A&A, 534, A18
Mombarg, J. S. G., Dotter, A., Van Reeth, T., et al. 2020, ApJ, 895, 51
Morel, P. & Lebreton, Y. 2008, Ap&SS, 316, 61
Nsamba, B., Campante, T. L., Monteiro, M. J. P. F. G., et al. 2018, MNRAS, 477, 5052
Nsamba, B., Moedas, N., Campante, T. L., et al. 2020, MNRAS
Paxton, B., Bildsten, L., Dotter, A., et al. 2011, ApJS, 192, 3
Paxton, B., Cantiello, M., Arras, P., et al. 2013, ApJS, 208, 4
Paxton, B., Marchant, P., Schwab, J., et al. 2015, ApJS, 220, 15
Paxton, B., Schwab, J., Bauer, E. B., et al. 2018, ApJS, 234, 34
Paxton, B., Smolec, R., Schwab, J., et al. 2019, ApJS, 243, 10
Perraut, K., Borgniet, S., Cunha, M., et al. 2013, A&A, 559, A21
Perraut, K., Brandão, I., Cunha, M., et al. 2016, A&A, 590, A117
Perraut, K., Brandão, I., Mourard, D., et al. 2011, Astronomy & Astrophysics, 526, A89
Perraut, K., Cunha, M., Brandão, I., et al. 2015, A&A, 579, A85
Perraut, K., Cunha, M., Romanovskaya, A., et al. 2020, A&A, 642, A101
Petit, V., Keszthelyi, Z., MacInnis, R., et al. 2017, MNRAS, 466, 1052
Power, J., Wade, G. A., Hanes, D. A., Aurier, M., & Silvester, J. 2007, in Physics of Magnetic Stars, ed. I. I. Romanyuk, D. O. Kudryavtsev, O. M. Neizvestnaya, & V. M. Shapoval, 89–97
Quitral-Manosalva, P., Cunha, M. S., & Kochukhov, O. 2018, MNRAS, 480, 1676
Rendle, B. M., Buldgen, G., Miglio, A., et al. 2019, MNRAS, 484, 771
Richard, O., Michaud, G., & Richer, J. 2001, ApJ, 558, 377
Richer, J., Michaud, G., & Turcotte, S. 2000, ApJ, 529, 338
Rogers, F. J. & Nayfonov, A. 2002, ApJ, 576, 1064
Romanovskaya, A., Ryabchikova, T., Shulyak, D., et al. 2019, MNRAS, 488, 2343
Royer, F., Grenier, S., Baylac, M. O., Gómez, A. E., & Zorec, J. 2002, A&A, 393, 897
Saio, H. & Gautschy, A. 2004, MNRAS, 350, 485
Schneider, F. R. N., Ohlmann, S. T., Podsiadlowski, P., et al. 2020, MNRAS, 495, 2796
Semenova, E., Bergemann, M., Deal, M., et al. 2020, A&A, 643, A164
Serenelli, A. M. 2010, Ap&SS, 328, 13
Shulyak, D., Ryabchikova, T., Mashonkina, L., & Kochukhov, O. 2009, A&A, 499, 879
Sikora, J., Wade, G. A., Power, J., & Neiner, C. 2019, MNRAS, 483, 3127
Sousa, S. G. & Cunha, M. S. 2008, MNRAS, 386, 531
Stift, M. J. & Alecian, G. 2016, MNRAS, 457, 74
Théado, S., Vauclair, S., & Cunha, M. S. 2005, A&A, 443, 627
ud-Doula, A. & Owocki, S. P. 2002, ApJ, 576, 413
ud-Doula, A., Owocki, S. P., & Townsend, R. H. D. 2008, MNRAS, 385, 97
ud-Doula, A., Owocki, S. P., & Townsend, R. H. D. 2009, MNRAS, 392, 1022
Uesugi, A. & Fukuda, I. 1970, Catalogue of rotational velocities of the stars
van Leeuwen, F. 2007, Astronomy & Astrophysics, 474, 653
Verma, K., Raodeo, K., Basu, S., et al. 2019, MNRAS, 483, 4678
Weiss, W. W., Fröhlich, H. E., Kallinger, T., et al. 2020, A&A, 642, A64
Wolff, S. C. 1967, ApJS, 15, 21
Wolff, S. C. 1968, PASP, 80, 281

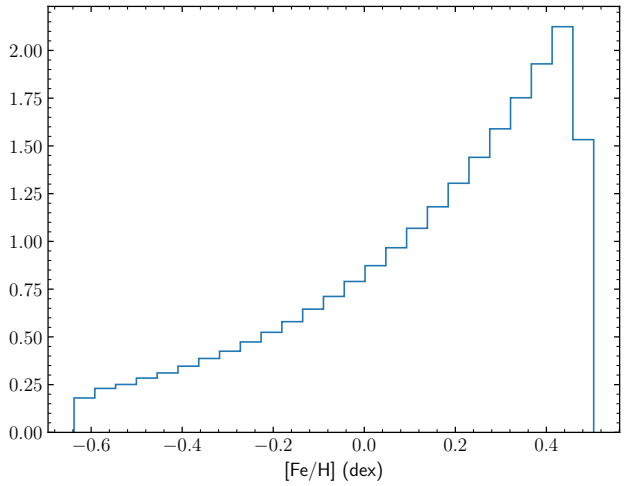

Fig. A.1. Distribution of [Fe/H] in a dense Cartesian grid (300 equally spaced values of $Y_{\rm ini}$ and $Z_{\rm ini}$) with $Y_0 = [0.242; 0.292]$ and $Z_{\rm ini} = [0.0031; 0.0381]$ using an AGSS09 solar composition.

Appendix A: [Fe/H] distribution in the grid

Figure A.1 shows the distribution of [Fe/H] in a dense Cartesian grid with $Y_0 = [0.242; 0.292]$ and $Z_{\rm ini} = [0.0031; 0.0381]$.

Appendix B: HD128898

Probability density functions for mass, age, X_c, $Y_{\rm ini}$, $Y_{\rm ini}$ and [Fe/H] of HD 128898.

Appendix C: Mass, age, X_c and [Fe/H] distributions

Probability density functions for four parameters of the stars of the sample (except HD 24712 and HD 128898), considering the non-seismic constraints (radius and luminosity).

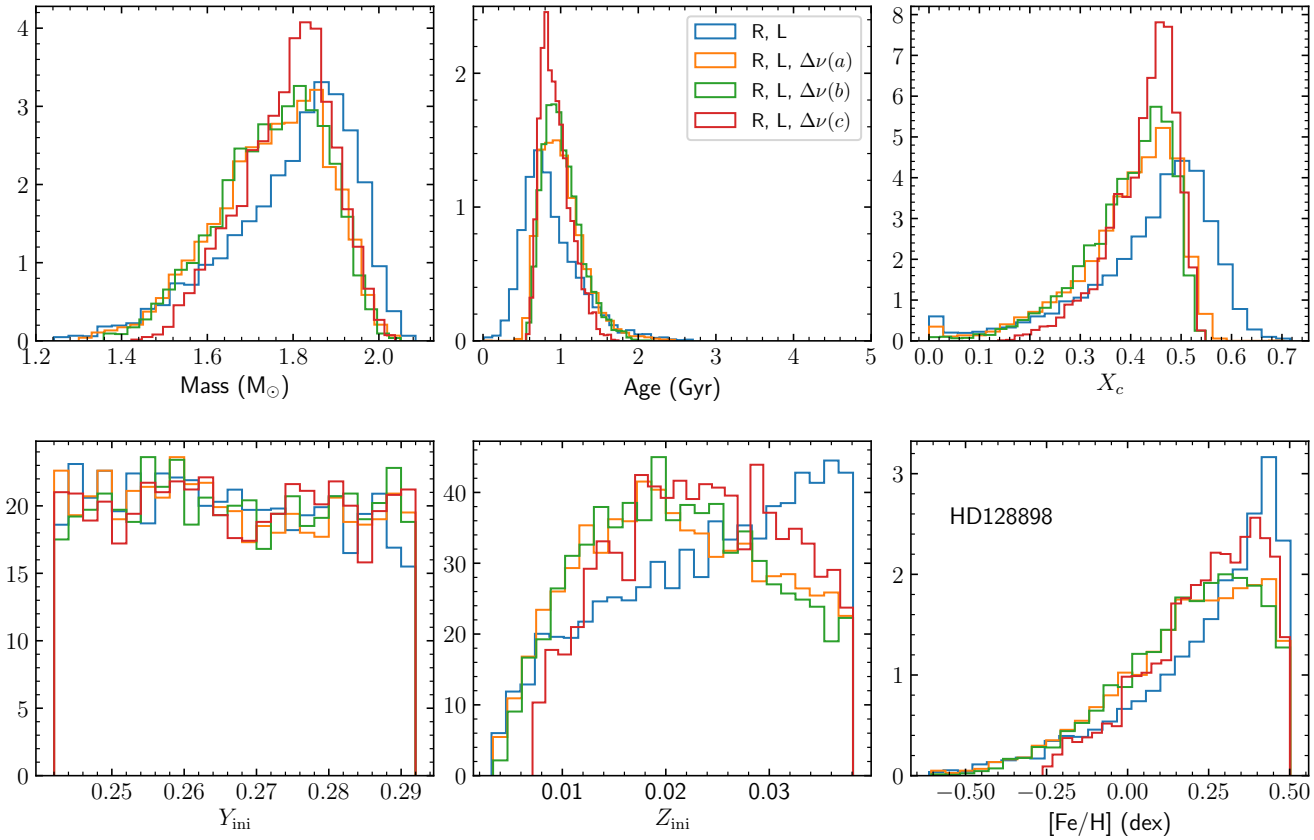

Fig. B.1. Same figure as Fig. 3 for HD HD128898.

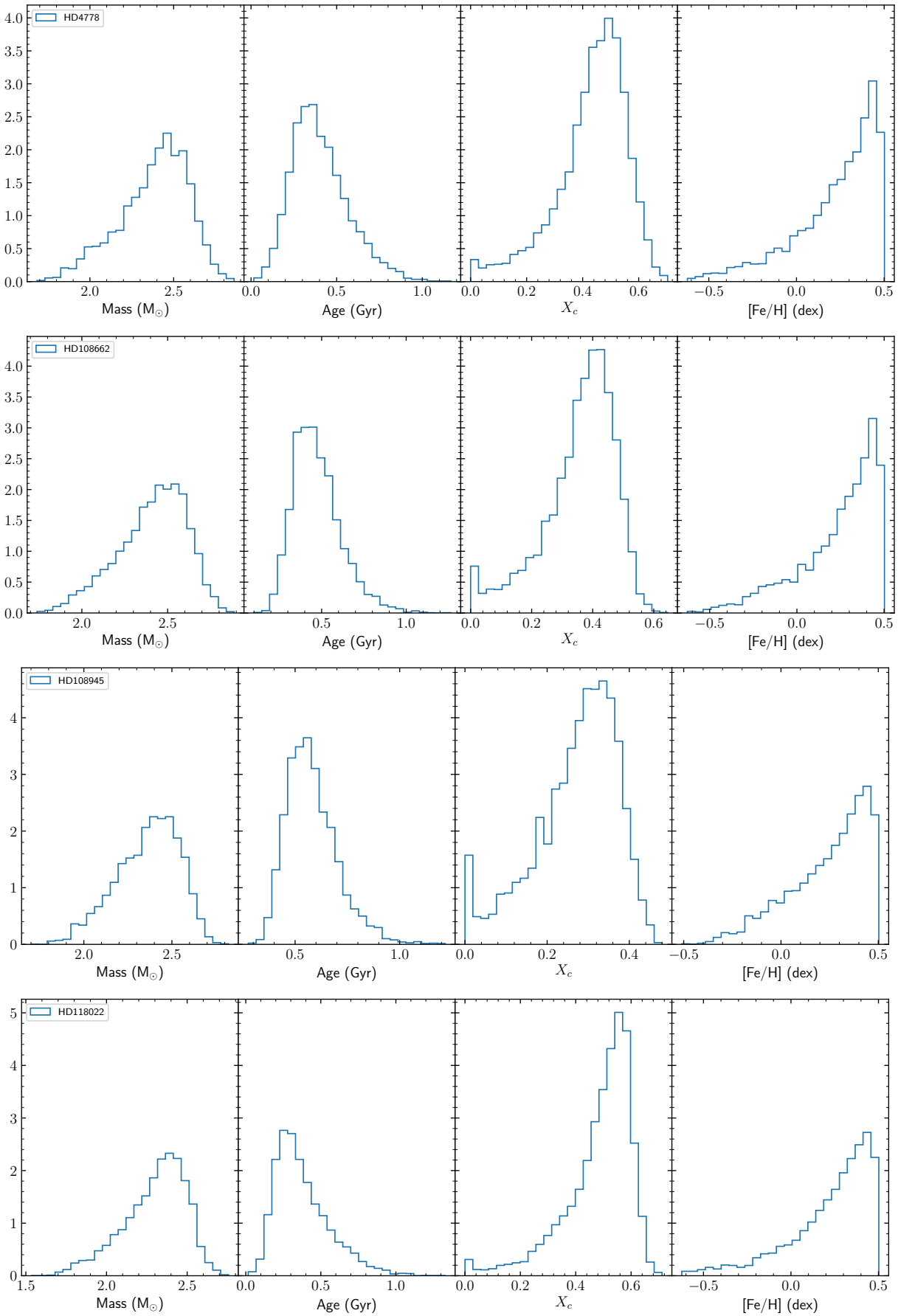

Fig. C.1. Probability density functions for the mass, radius, hydrogen mass fraction in the core (X_c) and [Fe/H] for HD 4778, HD 108662, HD 108945 and HD 118022.

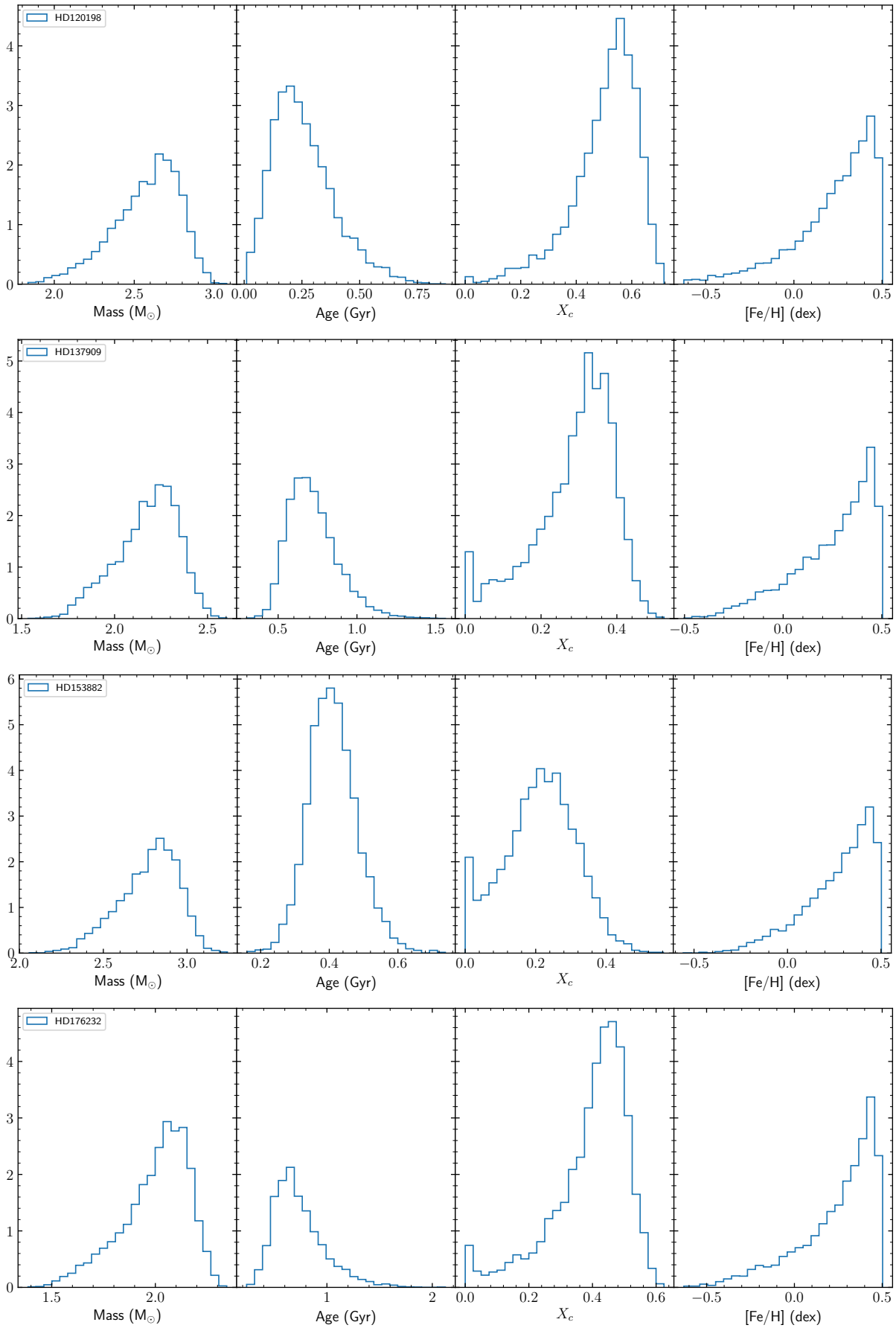

Fig. C.2. Same legend as Fig. C.1 for , HD 12019, HD 137909 HD 153882 and HD 176232.

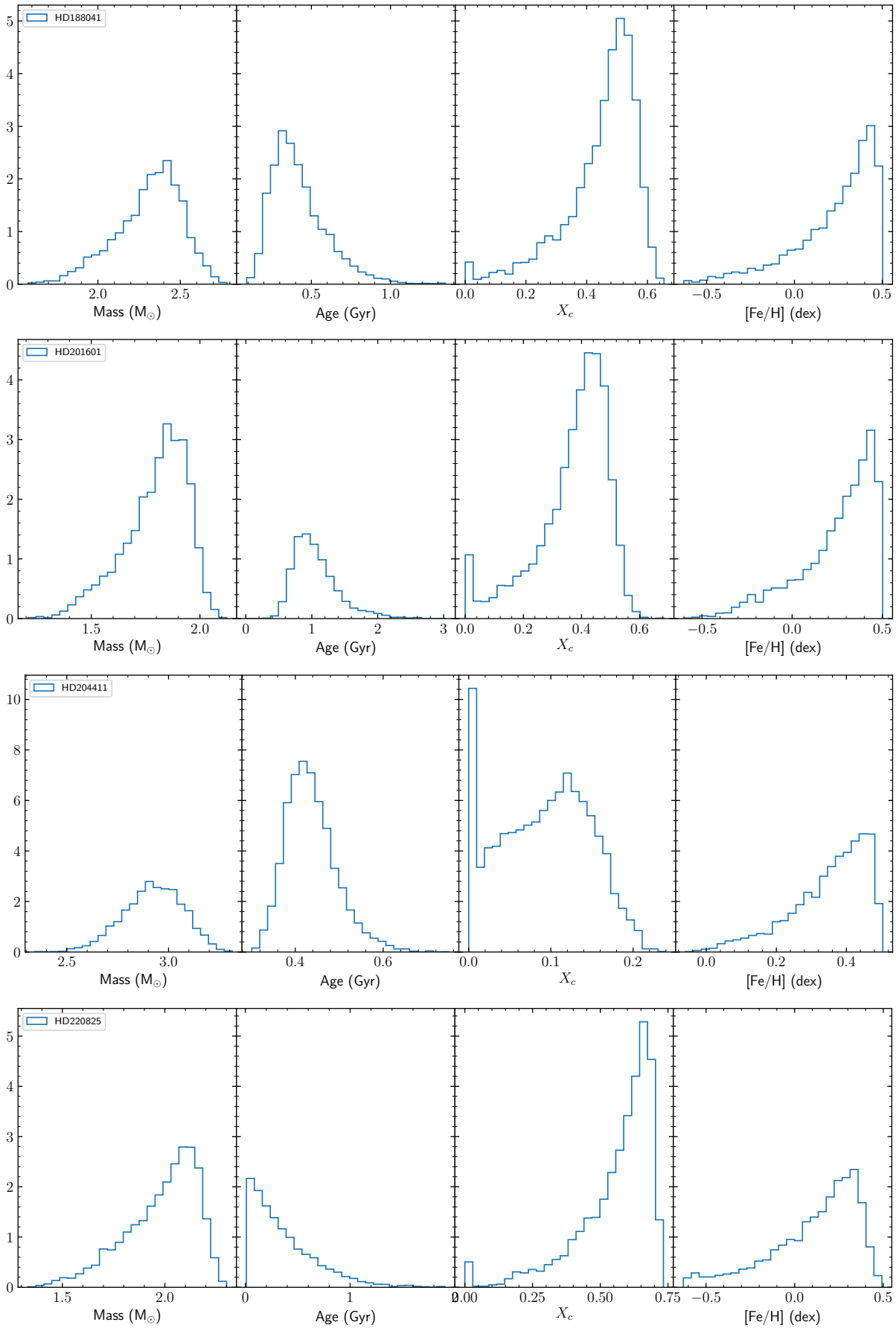

Fig. C.3. Same legend as Fig. C.1 for , HD 188041,HD 201601, HD 204411 and HD 220825 .